

Thermodynamic and dynamic contributions to future changes in summer precipitation over Northeast Asia and Korea: a multi-RCM study

Donghyun Lee¹ · Seung-Ki Min¹  · Jonghun Jin¹ · Ji-Woo Lee² · Dong-Hyun Cha³ · Myoung-Seok Suh⁴ · Joong-Bae Ahn⁵ · Song-You Hong⁶ · Hyun-Suk Kang⁷ · Minsu Joh⁸

Received: 18 January 2016 / Accepted: 1 February 2017 / Published online: 23 March 2017
© Springer-Verlag Berlin Heidelberg 2017

Abstract This study examines future changes in precipitation over Northeast Asia and Korea using five regional climate model (RCM) simulations driven by single global climate model (GCM) under two representative concentration pathway (RCP) emission scenarios. Focusing on summer season (June–July–August) when heavy rains dominate in this region, future changes in precipitation and associated variables including temperature, moisture, and winds are analyzed by comparing future conditions (2071–2100) with a present climate (1981–2005). Physical mechanisms are examined by analyzing moisture flux convergence at 850 hPa level, which is found to have a close relationship to precipitation and by assessing contribution of thermodynamic effect (TH, moisture increase due to warming) and dynamic effect (DY, atmospheric circulation change) to changes in the moisture flux convergence. Overall background warming and moistening are projected over the Northeast Asia with a good inter-RCM agreement,

indicating dominant influence of the driving GCM. Also, RCMs consistently project increases in the frequency of heavy rains and the intensification of extreme precipitation over South Korea. Analysis of moisture flux convergence reveals competing impacts between TH and DY. The TH effect contributes to the overall increases in mean precipitation over Northeast Asia and in extreme precipitation over South Korea, irrespective of models and scenarios. However, DY effect is found to induce local-scale precipitation decreases over the central part of the Korean Peninsula with large inter-RCM and inter-scenario differences. Composite analysis of daily anomaly synoptic patterns indicates that extreme precipitation events are mainly associated with the southwest to northeast evolution of large-scale low-pressure system in both present and future climates.

Keywords Regional climate models · Precipitation · Northeast Asia · Korea · RCP scenarios · Moisture flux convergence

✉ Seung-Ki Min
skmin@postech.ac.kr

¹ Division of Environmental Science and Engineering, Pohang University of Science and Technology, Pohang, Korea

² Lawrence Livermore National Laboratory, Livermore, USA

³ Ulsan National Institute of Science and Technology, Ulsan, Korea

⁴ Kongju National University, Gongju, Korea

⁵ Pusan National University, Busan, Korea

⁶ Korea Institute of Atmospheric Prediction Systems, Seoul, Korea

⁷ National Institute of Meteorological Sciences, Jeju, Korea

⁸ Korea Institute of Science and Technology Information, Daejeon, Korea

1 Introduction

The observed intensification of extreme precipitation on global and continental scales has been reported by a number of studies (e.g., Trenberth et al. 2003; Min et al. 2011; Zhang et al. 2013). As documented in the 5th assessment report of the Intergovernmental Panel on Climate Change (IPCC 2013), most regions over the world are very likely to experience more frequent and enhanced extreme precipitation events in the future, which will exert devastating impacts on human society like economy and health as well as on the ecosystem. In general, large-scale extreme precipitation changes can be well scaled by thermodynamic effect, which represents atmospheric moisture increase as

warming (Allen and Ingram 2002; Held and Soden 2006; Kharin et al. 2007; O’Gorman and Schneider 2009; Min et al. 2011). However, the importance of dynamic effect has been identified as well, which involves changes in atmospheric circulation, on regional and local changes in precipitation and its extremes (e.g., Emori and Brown 2005; Kendon et al. 2010; Endo and Kitoh 2014; Freychet et al. 2015).

Many studies have utilized Global Climate Model (GCM) simulations to study future changes in large-scale precipitation (e.g., Min et al. 2006; Seager et al. 2010; Seo et al. 2013; Lee and Wang 2014). Previous GCM studies suggested that while frequency and intensity in extreme precipitation are expected to increase, total precipitation is generally projected to increase or decrease depending on regions and seasons, indicating larger uncertainties. However, fundamental information required to prepare for climate change adaptation strategies is on smaller-scale changes, particularly reliable projections of extreme events which are basically short-term and localized phenomena. In order to project future climate changes on higher resolutions, downscaling studies have been conducted using regional climate model (RCM) simulations and also statistical approaches (Murphy 1999; Wilby et al. 1998; Giorgi et al. 2009). The benefit of RCM comes from its capability of local simulations on unprecedented high resolution given available computing resources (e.g., Laprise 2008). In this way, dynamic downscaling can provide useful details on space–time climate change patterns when compared to GCMs, so-called added value (Hong and Kanamitsu 2014; Lee and Hong 2014). Recently, Di Luca et al. (2015) have reviewed current issues on added value in dynamic downscaling, noting that “added value can be true or false depending on the point of view”. They suggested assessing added value based on “physically meaningful causal chain” rather than “focusing on simple statistics”.

Global monsoon studies (e.g., Kitoh et al. 2013) projected future increase in damages due to heavy rainfall events over monsoon regions in warming climate. One of the monsoon regions, East Asia including Korea is projected to experience more extreme events in the future, and model evaluations of and future changes in precipitation characteristics have been actively carried out (e.g., Oh et al. 2013, 2016; Lee et al. 2014; Im et al. 2015; Cha et al. 2015, 2016; Hong and Ahn 2015; Park et al. 2016; Ahn et al. 2016; Choi et al. 2016). Future projections commonly suggested the increase in heavy precipitation frequency and/or intensity under global warming. Although natural internal variability modes can affect climate extremes, the apparent greenhouse warming is expected to induce increase in hot extremes and heavy rain events over East Asia and Korea (Min et al. 2015 and references therein). Nevertheless, for the Northeast Asia and Korea, studies have been very

limited for understanding physical mechanisms for precipitation change and assessing associated uncertainties arising from different scenarios and models.

The aim of this study is to examine changes in precipitation over Northeast Asia and Korea during summer (June–July–August, JJA) using multi-RCMs. Physical mechanisms are investigated by analyzing relative contributions from thermodynamic (moisture increase due to warming) and dynamic (atmospheric circulation change) effects, which are based on a simplified version of moisture budget analysis at 850 hPa level. Inter-RCM differences in thermodynamic and dynamic terms are also examined to understand factors affecting future projection uncertainties. Two emission scenarios are compared to examine the influence of external radiative forcing on future changes. Moreover, focusing on South Korea, future changes in precipitation characteristics like intensity and frequency distributions are examined. Weather system patterns associated with extreme precipitation events over Korea are also investigated using composite analysis for the present and future conditions.

Considering that changes in extreme summer-season precipitation over Korea are closely related to changes in East Asia summer monsoon (EASM, Wang et al. 2001; Kusunoki et al. 2006; Seo et al. 2013; Kitoh et al. 2013; Lee et al. 2014; Matsumura et al. 2015; Ham et al. 2015), understanding future changes in summer precipitation over this small domain can provide useful insights to and implications for larger-scale features of East Asian climate changes.

This paper is structured as follows. In Sect. 2, data from observations and five RCMs are described, and analysis methods are explained including moisture flux convergence analysis and composite analysis. Results are provided in Sect. 3 for Northeast Asian climate and South Korean precipitation characteristics and extremes. Summary and discussions are given in Sect. 4.

2 Data and methods

2.1 Data

APHRODITE data (Asian Precipitation-Highly-Resolved Observational Data Integration Towards Evaluation of water resources, Yatagai et al. 2012) are used as observations for precipitation (hereinafter referred to as PR), which are station-based daily dataset with high resolution of 0.25° longitude \times 0.25° latitude. ERA-Interim data (Dee et al. 2011) are used for atmospheric variables such as surface specific humidity and temperature, horizontal winds, and specific humidity at 850 hPa level. Northeast Asian and South Korean domains are defined as latitude-longitude

boxes of 30°N–44°N and 117°E–138°E, and of 34°N–39°N and 125.5°E–130°E, respectively.

Five RCMs (HadGEM3-RA, RegCM4, SNURCM, WRF, and GRIMs) are analyzed in this study. Table 1 lists the models with their configurations such as resolutions, cloud physics, land surface, radiation, and spectral nudging. These five RCMs were driven by one boundary condition obtained from the HadGEM2-AO GCM (Baek et al. 2013; Suh et al. 2016). Given the single GCM forcing, different results across RCMs are likely to be due mainly to their differences in RCM physics. Especially, five RCMs use different convective parameterization schemes, which will have strong influence on precipitation. Spectral nudging is applied to three RCM members, except HadGEM3-RA and WRF. Usually large-scale nudging improves the RCM simulations by revising small-scale circulations and eliminating spurious influence of the lateral boundaries on large-scale circulation inside the domain (Miguez-Macho et al. 2004; Kanamaru and Kanamitsu 2007; Laprise 2008; Hong and Chang 2012). However, given small number of models, we do not find systematic differences between two model groups with and without spectral nudging (see below), possibly indicating important influence of different model physics such as convective parameterization schemes (e.g., Yang et al. 2012). To consider different grid numbers among RCMs, we use the common domain (180 grid points in latitude × 200 grid points in longitude) excluding buffer zones (Table 1). For more details on model configurations, refer to Suh et al. (2016).

Five RCMs were integrated to conduct a present day simulation for 1979–2010 and future experiments for 2019–2100 under different RCP scenarios (Suh et al. 2016). To analyze future changes over the Northeast Asia, we compare model outputs from a present-day 25-year period (1981–2005) driven by GCM historical experiment (HIST, based on the observed forcing) with those from late twenty-first century 30 years (2071–2100) downscaled under RCP4.5 and RCP8.5 scenarios. To obtain overall RCM results, we construct MME

(multi-model ensemble) means for each RCP scenario, which are simple arithmetic averages of five RCMs. We interpolate all RCM data (12.5 × 12.5 km) onto the same grids of APH-RODITE before analysis. In order to assess the influence of GCM boundary forcing, HadGEM2-AO results are also used on its original resolution (1.875° longitude × 1.25° latitude).

2.2 Moisture flux convergence analysis

In order to analyze roles of thermodynamic effect (due to moisture increase due to warming) and dynamic effect (due to changes in atmospheric circulation) in future rainfall changes, we conduct a moisture flux convergence analysis which is a simplified form of moisture budget analysis for a single atmospheric level. We select 850 hPa because daily wind and moisture data are only available at this level for all RCMs. Before examining changes in horizontal moisture flux convergence (hereinafter, HMFC) at single vertical level, we consider linearized formulation used by Seager et al. (2010) and Endo and Kitoh (2014) as follows:

$$\delta PR = \delta E + \delta TH + \delta DY + \delta TE + Res \tag{1}$$

$$\delta TH = - \frac{1}{\rho_w g} \int_0^{P_s} \nabla \cdot (\bar{\mathbf{u}}_{20} [\delta \bar{q}]) dp \tag{2}$$

$$\delta DY = - \frac{1}{\rho_w g} \int_0^{P_s} \nabla \cdot ([\delta \bar{\mathbf{u}}] \bar{q}_{20}) dp \tag{3}$$

$$\delta TE = - \frac{1}{\rho_w g} \int_0^{P_s} \nabla \cdot \delta (\overline{\mathbf{u}'q'}) dp \tag{4}$$

$$\delta(\cdot) = (\cdot)_{21} - (\cdot)_{20} \tag{5}$$

where PR is precipitation, E is evaporation from the surface, g is the acceleration of gravity, ρ_w is the density of water, \mathbf{u} is the horizontal wind vector, q is the specific

Table 1 List of five RCMs used in this study (adopted from Suh et al. 2016)

Model	HadGEM3-RA	RegCM4	SNURCM	WRF	GRIMs
# of grid points (Lat. x Lon.)	180 × 200	180 × 200	180 × 200	180 × 201	182 × 201
Vertical level	Hybrid-38	σ -23	σ -24	Eta-28	σ -28
Dynamic framework	Non-hydrostatic	Hydrostatic	Non-hydrostatic	Non-hydrostatic	Hydrostatic
Convection scheme	Revised mass flux scheme	MIT-Emanuel	Karin-Fritsch II	Karin-Fritsch	SAS + CMT
Land surface	MOSES-II	CLM3.5	CLM3.0	Noah	OML-climatology value
Radiation scheme	Generalized 2-stream	CCM3	CCM2	CAM	GSFC
Spectral nudging	No	Yes	Yes	No	Yes
References	Hewitt et al. (2011)	Giorgi et al. (2012)	Lee et al. (2004)	Skamarock et al. (2005)	Hong et al. (2013)

humidity, and p is the pressure. Overbars indicate climatological monthly means (seasonal results are obtained by averaging monthly results). Subscripts 20 and 21 indicate 20th-century and 21st-century values, respectively. Moisture budget concept allows direct comparison among precipitation, evaporation, and vertical integrated MFC (VIMFC) based on the same unit (mm/day). The VIMFC terms influenced by changes in specific humidity and by in mean circulation become thermodynamic (δTH) and dynamic (δDY) components, respectively. Mathematically, δTH and δDY terms are integrated HMFC from surface to top of atmosphere given future changes in specific humidity and horizontal wind, respectively. Transient eddy (δTE) term is calculated by using daily output, apart from monthly mean for twentieth and twenty-first century, respectively. Residual (Res) term is composed of nonlinearity in moisture flux convergence i.e. $\delta\text{NL} = [\nabla \cdot (\delta\bar{u}\delta\bar{q})]$, surface quantities and computation errors [see Seager et al. (2010) for details]. Res term is usually neglected due to relatively small contribution (Seager et al. 2010; Endo and Kitoh 2014). On the other hand, future changes in evaporation seems to play a secondary role in determining PR changes, but previous studies (e.g., Gao et al. 2012) suggested that RCMs and even GCMs cannot simulate moisture balance properly, sometimes yielding non-negligible residuals between PR-E and VIMFC, which makes it difficult to assess moisture budget and recycling ratio.

Similarly to VIMFC, taking one specific level of 850 hPa from the vertical integrals, HMFC change at 850 hPa level (δHMFC_{850}) can be partitioned into four terms:

$$\delta\text{HMFC}_{850} = \delta\text{TH}_{850} + \delta\text{DY}_{850} + \delta\text{TE}_{850} + \delta\text{NL}_{850} \quad (6)$$

$$\delta\text{TH}_{850} = -\nabla \cdot (\bar{u}_{20}[\delta\bar{q}])_{850} \quad (7)$$

$$\delta\text{DY}_{850} = -\nabla \cdot ([\delta\bar{u}]\bar{q}_{20})_{850} \quad (8)$$

$$\delta\text{TE}_{850} = -\nabla \cdot \delta(\overline{u'q'})_{850} \quad (9)$$

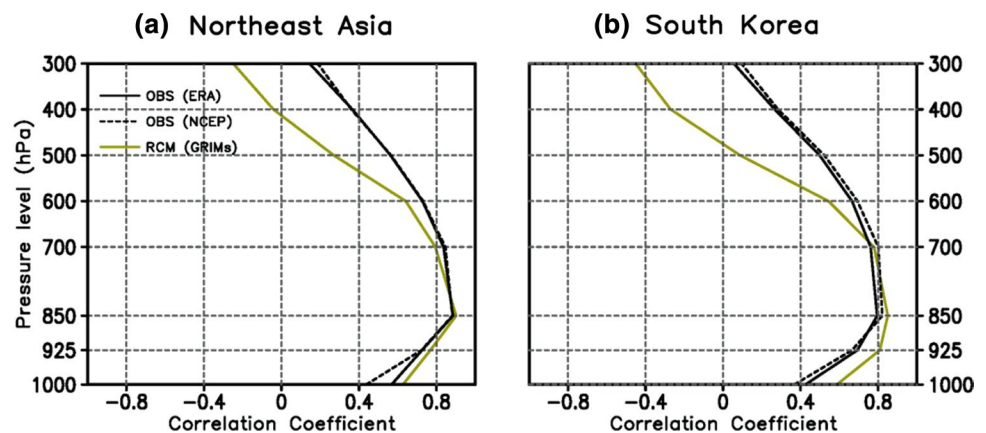
$$\delta\text{NL}_{850} = -\nabla \cdot (\delta\bar{u}\delta\bar{q})_{850} \quad (10)$$

where subscript 850 indicates variable at 850 hPa. The terms of δHMFC_{850} and δTE_{850} are calculated by using daily outputs, and the others are computed from monthly outputs. Limitation may exist in this approach due to the omission of vertical integration of whole atmospheric level (Seager et al. 2010; Seager and Henderson 2013; Endo and Kitoh 2014), making it hard to directly compare precipitation change (mm/day) and HMFC_{850} change ($\text{g/kg/s}/10^5$). In this respect, we have made a simple comparison of HMFC at different pressure levels with VIMFC averaged over the Northeast Asia and South Korea using available RCM data (GRIMs) and ERA-Interim and NCEP/NCAR reanalyses (see below) during JJA for 1979–2005 (Fig. 1). Strongest correlation ($r > 0.8$) is found at 850 hPa level in both RCM and reanalyses results, supporting that HMFC_{850} can represent VIMFC reasonably well in this region. Also, an analysis of inter-RCM relation suggests that HMFC_{850} change can be used as a good indicator of precipitation change over this region (see below for details).

2.3 Precipitation frequency and intensity

Precipitation characteristics during summer (JJA) are analyzed using daily precipitation averaged over South Korea. Frequency of daily precipitation is obtained for different ranges with 10 mm/day intervals. Each frequency is standardized by total summer days, in order to compare frequency change despite of different climate years (present: 25 years, future: 30 years) and different calendar days across models (360 days: HadGEM3-RA, RegCM4 and GRIMs, 365 days: SNURCM and WRF). Intensity is measured based on percentiles with 10 bins of every 10 percentiles. The top 10 percentiles are additionally divided into 10 bins of 1% of each for details following Freychet et al. (2015). In this analysis, we consider only wet days with

Fig. 1 Vertical distribution of correlation coefficients between horizontal moisture flux convergence (HMFC) at each pressure level from 1000 to 300 hPa and vertical integrated moisture flux convergence (VIMFC) averaged over **a** Northeast Asia and **b** South Korea obtained from JJA (June–July–August) daily data during 1979–2005 from GRIMs HIST simulation (yellow) and ERA-Interim (black solid) and NCEP/NCAR (black dashed) reanalyses



daily precipitation averaged over South Korea being more than 0.1 mm/day.

2.4 Composite analysis

Composite analysis is used to study spatial patterns associated with extreme precipitation events over South Korea. Here, extreme precipitation events are defined as days with precipitation amounts over the 95th percentile intensity (hereinafter PR95) during summer estimated from wet days (with precipitation averaged over South Korea more than 0.1 mm/day). For the days having precipitation more than the threshold, we calculate averages of fields to obtain spatio-temporal composite patterns for equivalent potential temperature (θ_e), specific humidity, horizontal winds, and HMFC at 850 hPa level and precipitation. Also, we investigate weather system evolutions related to South Korea extreme precipitation by compositing those variables from 2 days before to 1 day after extreme precipitation events. To evaluate modeled synoptic pattern, observations are also composited using two reanalysis data sets from ERA-Interim (0.25° lon × 0.25° lat version, Dee et al. 2011) and NCEP/NCAR R1 (2.5° lon × 2.5° lat, Kalnay et al. 1996) to take account of possible uncertainty in reanalyses. Two reanalyses provide generally consistent results despite of different resolutions, so we show only ERA-Interim results below.

3 Results

3.1 Summer mean precipitation over Northeast Asia

To understand model skills and future changes in terms of background large-scale conditions, we analyze Northeast Asian summer (JJA) climate simulated by RCMs for the present and future periods. In order to check significance in model biases and future projections, considering the small number of RCMs, we have simply checked inter-model agreement in sign (i.e. significant if more than four models out of five have same sign of bias or change), which is commonly applied (e.g., Endo and Kitoh 2014; He and Zhou 2015).

3.1.1 RCM performance

Previous studies evaluated same RCMs in terms of surface air temperature and precipitation (Park et al. 2016; Suh et al. 2016; Oh et al. 2016). Although systematic biases exist over some areas such as cold and dry bias over South Korea during JJA, high-resolution RCMs were found to provide better skills in reproducing the observed smaller scale patterns than the driving GCM over the Northeast

Asia (Lee and Hong 2014; Suh et al. 2016; Oh et al. 2016). Building on previous studies, since our analyses focus on precipitation and 850 hPa moisture flux convergence, here we further evaluate RCM performances based on JJA mean precipitation and low-level humidity, winds, and temperature (Fig. 2). RCMs display systematic biases in 850 hPa temperatures, which resemble surface temperature biases (Suh et al. 2016). A warm bias appears over land, particularly the northeast part of the domain (about +0.7 K), and a cold bias is seen over the East Sea (about −0.5 K). RCMs generally underestimate low level specific humidity (up to −0.6 g/kg) over South Korea, which is consistent with dry bias in precipitation. Southwesterly winds are also underestimated by RCMs, and an easterly wind bias (around −3 m/s) prevails. Similar wind bias occurs in the driving GCM (not shown), representing large influence of GCM boundary forcing. The spectral nudging was implemented in three RCMs (Table 1), and bias patterns of individual RCMs confirm the transfer of GCM wind bias into those RCMs (not shown).

3.1.2 Future climate projections

Future projections simulated by five RCM-MME are displayed in Fig. 3. Changes in sea surface temperature (SST), surface air temperature (TAS), and specific humidity at surface (q_s) are expected to increase everywhere with larger amplitudes in the RCP8.5 scenario than in the RCP4.5 scenario. This represents that RCM temperature and humidity responses are majorly governed by the radiative forcing change due to corresponding greenhouse gas increases. Inter-RCM relationship is examined between domain averaged surface air temperature and specific humidity with two RCP projections combined (Fig. 4a). Although only five RCMs are available, result suggests that Clausius–Clapeyron (C–C) relationship (about 7% moisture increase per 1 °C warming) holds in this region, implying that RCMs projecting warmer conditions tend to predict more increase in surface moisture. Regression slopes are 6.6%/°C and 7.2%/°C for RCP4.5 and RCP8.5 scenarios, respectively. A similarly strong C–C relationship is seen at 850 hPa level (not shown), indicating robust response in moisture following temperature increases in these downscaled results.

Results for future PR changes (Fig. 5, bottom panel) show weaker inter-RCM agreement (with large white areas indicating inter-model disagreement in the sign of future changes), compared to those for temperature and moisture (Fig. 3). PR increases prevail but PR decrease is also projected over some areas such as the central part of the Korea peninsula, particularly, in the RCP 4.5 scenario. Inter-model relationship of hydrological sensitivity (% change in PR per 1 °C warming) also shows large inter-RCM uncertainty (Fig. 4b). It is interesting to see that the slope

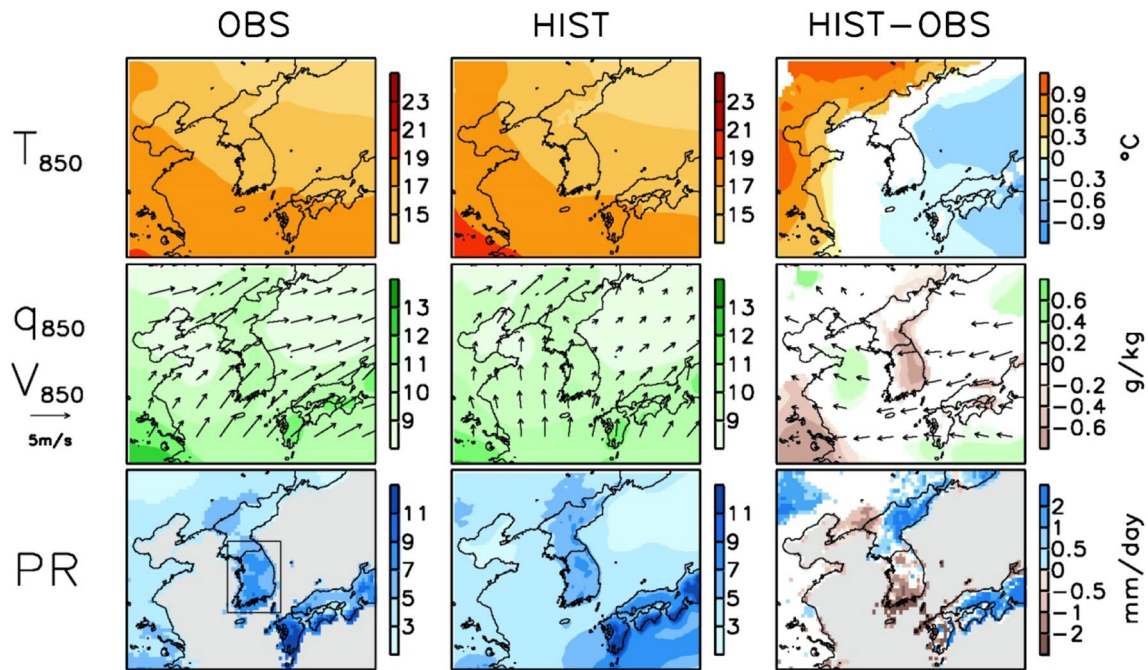


Fig. 2 Spatial distributions of observed climatology (*left*), RCM-MME climatology (*middle*), and RCM-MME bias (*right columns*) from historical (HIST) experiments during 1981–2005 for JJA mean temperature at 850 hPa (T_{850}), specific humidity at 850 hPa (q_{850} , shading) with horizontal winds (V_{850} , vectors), and precipita-

tion (PR). Biases are only displayed for areas with good inter-RCM agreement (*color shadings*, at least four models out of five agree on the sign of bias). *Grey colors* in PR depict missing data areas in the APHRODITE observations. *Black box* on the observed PR represents South Korean domain

of hydrological sensitivity of summer mean precipitation ($3\%/^{\circ}\text{C}$) over this region is similar to those estimated for a larger East Asian area (Park et al. 2016) and also for the globe (Held and Soden 2006; Kharin et al. 2007) despite of statistically non-significant results. In this regard, global mean precipitation changes are known to be controlled by the tropospheric energy balance, not by moisture availability, which leads to reduced upward latent heat flux from surface under greenhouse warming (Allen and Ingram 2002; Stephens and Ellis 2008; Allan 2009; IPCC 2013). But, regional hydrological sensitivity may contain uncertainties related to the atmospheric circulation response under warming (e.g. Deser et al. 2014; Endo and Kitoh 2014). Note that despite of non-significant precipitation response to temperature, relationship between precipitation and HMFC850 change shows statistically significant results as we discuss below (Sect. 3.1.3).

Figure 5 illustrates spatial patterns of future changes in temperature, humidity, and horizontal winds at 850 hPa level projected by five RCMs. Note that PR changes are presented here again but in the unit of mm/day (% change in Fig. 3) for better comparison with moisture amount. Under both RCP scenarios, PR is predicted to increase over most part of the Northeast Asian domain with stronger increases over the South Sea (or northern East China Sea) and Kyushu area. Both RCP scenarios identically project

more warming of lower troposphere on higher latitudes resulting in the weakening of future temperature gradient over Northeast Asia, resembling the warming patterns at the surface (Fig. 3). Moisture at 850 hPa level is also projected to increase everywhere with stronger amplitudes over the southern oceanic areas in both scenarios (note slight difference from the surface moisture change patterns in Fig. 3, which show % change).

Unlike temperature and moisture, horizontal low-level winds exhibit different changes between scenarios (Fig. 5). In the RCP4.5 scenario, anomalous cyclonic circulation prevails over the East Sea and north-easterly winds pass through the Korean Peninsula relative to the present-day climate. In contrast, weak southerly flows appear over the ocean areas under the RCP8.5 scenario. These circulation changes are likely to be associated with corresponding changes in the North Pacific Subtropical High (hereinafter NPSH) in the driving GCM. Previous studies based on multiple GCM simulations found consistent north-westward expansion of the NPSH under global warming (e.g., Zhou et al. 2009; Li et al. 2012a, b; Seo et al. 2013). A simple analysis of circulation changes in the HadGEM2-AO simulations confirms the possible north-westward shift of the NPSH (Fig. 6). Here 1,500 m contour of 850 hPa geopotential height is used to indicate NPSH area (cf., Li et al. 2012a, b; Seo et al. 2013;

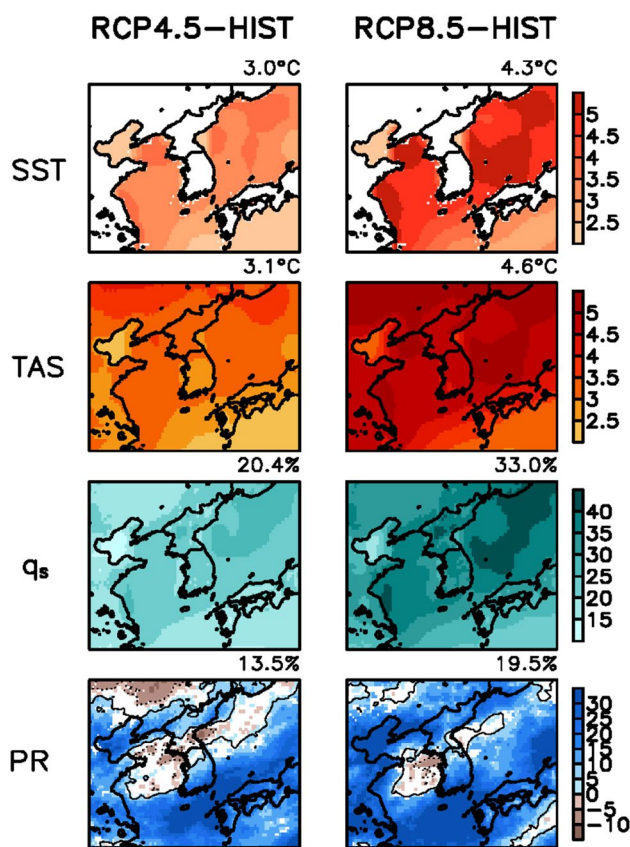


Fig. 3 Spatial distributions of RCM-MME future change patterns from RCP4.5 and RCP8.5 experiments for JJA mean SST (°C), surface air temperature (TAS, °C), surface specific humidity (q_s , %), and PR (%). Note that percentage changes relative to the present climatology are used for q_s and PR (%). Numbers on the top of each panel indicate domain averaged values. Results are only shown for areas with good inter-RCM agreement (color shadings, at least four models agree on the sign of change). Solid and dashed contours in PR indicate +5 and -5% changes, respectively

Lin and Chan 2015; Yun et al. 2015). In accord with RCM results, there are different circulation changes along the coastal area between two scenarios in the GCM. Around the Korean Peninsula, anomalous cyclonic circulation exists in the RCP 4.5 scenario, but anomalous easterly develops from the northern Japan. RCP8.5 scenario shows enhanced southerly flows in the south of the RCM domain and anomalous southwesterly flows in the north-west, consistent with RCM flow patterns. Note that despite of consistent increase in geopotential height, the atmospheric circulation responses associated with NPSH are different between RCP scenarios. This represents dynamical effect (i.e. atmospheric circulation changes) which contains a high proportion of unforced variability compared to GHG-forced signals (Deser et al. 2014).

3.1.3 Thermodynamic and dynamic contributions

In order to explore mechanisms responsible for the Northeast Asian precipitation changes, changes in low level moisture flux convergence are analyzed. For the large-scale changes over the Northeast Asia, $HMFC_{850}$ changes can well represent precipitation changes under global warming as shown in Fig. 4c ($r=0.87$). This strong $HMFC_{850}$ -PR relationship is also seen consistently from observations, RCMs, and GCM when using daily values of Northeast Asia area averages for the current period (not shown). Horizontal patterns of future changes in $HMFC_{850}$ and contribution of thermodynamic (TH) and dynamic (DY) terms, as described in Eqs. (6)–(10), are displayed in Fig. 7 (upper panel). $HMFC_{850}$ is predicted to increase mainly over land areas including the north-eastern part of the Korean Peninsula and the southern Japan. A decrease in $HMFC_{850}$ is expected in the northwestern and central part of the Korean Peninsula, where no change or slight decrease in precipitation is projected (Fig. 5). It can be seen that major contribution to the overall increase of $HMFC_{850}$ comes from TH effect. However, DY effect offsets the TH effect over some regions, particularly, along the central and northern inland area of the Korean Peninsula.

Figure 7 (bottom panel) compares domain averaged $HMFC_{850}$ changes and TH, DY, transient eddy (δTE), and non-linear (δNL) terms contributions for RCM-MME (bars) and individual RCMs (marks). While RCMs show a good agreement in TH effect with all RCMs projecting increases, DY effect exhibits mixture of positive and negative contributions across models and scenarios. In addition, inter-RCM uncertainty in $HMFC_{850}$ change seems to be affected more by inter-RCM difference in DY effect, particularly in the RCP8.5 scenario, which is well consistent with previous studies (Endo and Kitoh 2014). Due to the large inter-model uncertainty, two scenarios do not show noticeable differences in $HMFC_{850}$ changes as well as in TH and DY contributions. On the other hand, the influence of δTE and δNL terms is found to be negligible, consistent with the previous studies (Seager et al. 2010). We can further check possible influence of spectral nudging by comparing results between RCMs with and without spectral nudging (compare + marks with \circ marks in Fig. 7). Two groups do not show systematic differences in $HMFC$ and TH and DY contributions. As we pointed above, it is difficult to assess the impacts of spectral nudging given small number of model samples, and this result seems to suggest that inter-model uncertainty represents difference in model physics like convective parameterization schemes (e.g., Yang et al. 2012).

There are some differences in spatial patterns between $HMFC_{850}$ (Fig. 7) and precipitation (Fig. 5), representing possible limitation of our analysis based on single vertical

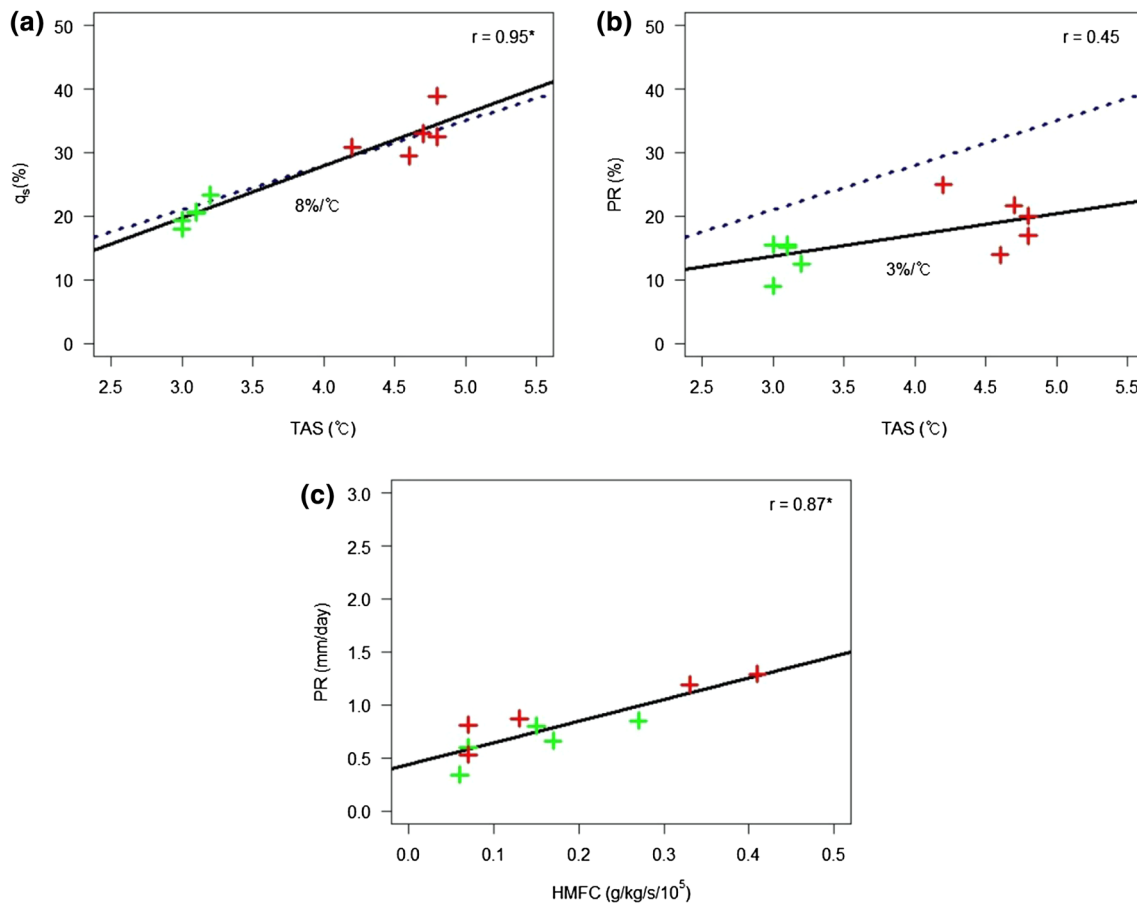


Fig. 4 Scatter plots for inter-model relationship of future changes between **a** surface specific humidity (q_s , %) and surface air temperature (TAS, °C), **b** mean PR (%) and TAS, and **c** PR (mm/day) and $HMFC_{850}$ ($g/kg/s/10^5$) from RCP4.5-HIST (green) and RCP8.5-HIST (red). All variables are values averaged over the Northeast Asian domain. Marks (+) indicate each RCM value and solid black lines

represents least square linear fit obtained from using all RCM results from two different scenarios (i.e. 10 values). Dashed lines in **a** and **b** represent the slope of Clausius–Clapeyron relationship ($7\%/^{\circ}C$) for comparison. Asterisk (*) indicates statistically significant correlation at 5% level based on two-sided *t*-test

level of 850 hPa. Evaporation and residual terms in the full vertical integrated moisture budget analysis as given in Eq. (1) will explain part of the difference (Seager et al. 2010; Endo and Kitoh 2014). However, if we exclude no-rain days, changes in low-level moisture flux convergence seem to better represent precipitation changes, which can be confirmed in the analysis of extreme precipitation (see below). Despite of the restrictions, our analysis provides mechanisms for mean precipitation change over the Northeast Asia with (1) the major contribution of TH effect to HMFC increase and (2) the local-scale offsetting DY effect to HMFC changes.

3.2 Summer precipitation characteristics in South Korea

Building on the analysis results on mean precipitation changes conducted above, in this section we examine

precipitation characteristics and mechanisms focusing on South Korea. Figure 8 (upper panel) shows histogram of daily precipitation averaged over South Korea for the present and future periods. Note that each frequency is standardized into % unit relative to total summer days as described in Sect. 2.3. Moreover, results with physical unit (days during JJA) are also provided by multiplying boreal summer days (92 days) to percentage frequency (%). Compared to the APHRODITE observations, RCMs on average simulate more frequent light rain events [$0.1 \sim 10$ mm; $+10.40\%$ ($+9.6$ days) estimated as model frequency (65.2 days) – observed frequency (55.6 days)] and less frequent moderate [$10 \sim 50$ mm; -3.12% (-2.9 days), relative to observed frequency (19.2 days)] and heavy rain frequency [>50 mm; -0.30% (-0.3 day), relative to observed frequency (1.0 day)]. The driving GCM results are also compared. Boundary GCM results are largely similar to RCMs [$+0.81\%$ (-0.7 day), -4.38% (-4.5 days), and -0.29%

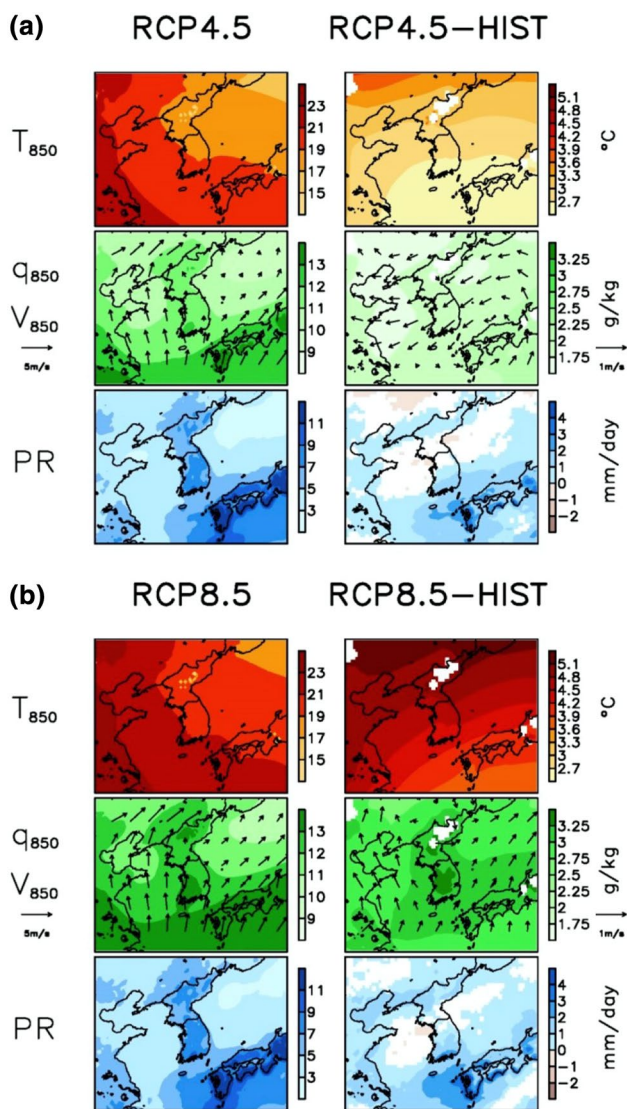


Fig. 5 **a** Spatial distributions of RCM-MME future climate (*left*) and change patterns (future – present; *right*) relative to historical period for JJA mean T_{850} , Q_{850} with horizontal winds (V_{850} , vectors), and PR from RCP4.5 scenario experiments. **b** Same as **a** except for RCP8.5 scenario experiments. In change patterns, *color shading* represents region where at least four RCMs (out of five) agree on the change sign

(–0.3 day) frequency biases for light, moderate, and heavy rains, respectively] but it fails in capturing extreme rain events (>80 mm) which can be reproduced by RCMs. Such extreme events are very rare in observation (3 days out of 2300 days, 0.13% chance), so the difference in probability of the event will not be statistically significant. However, this result is consistent with previous findings based on the same RCMs with 12.5 km resolution (Lee and Hong 2014; Oh et al. 2016) and with 50 km resolution (Park et al. 2016), suggesting a possible added value in dynamic down-scaling over GCM for extreme precipitation simulations.

Results from RCP4.5 and RCP8.5 scenarios suggest that frequency of the light rain slightly decreases by 0.8% and 1.6% for RCP4.5 and RCP8.5 relative to the present frequency but that frequency of heavy rain days increases relatively by 65% and 70% for RCP4.5 and RCP8.5 scenarios (Fig. 8). When looking at inter-RCM agreement in frequency changes in the future, good agreements are seen for the increase in frequency of heavy rain days irrespective of scenarios (at least four RCMs agree on change sign; not shown). Model uncertainty becomes, however, larger in the changes in moderate and light rain days under RCP4.5 scenario, for which less than half RCMs predict increase in some categories. Considerable differences in frequency changes exist between scenarios as well.

Distributions of daily precipitation intensity over South Korea during JJA from HIST and RCP scenarios are examined (Fig. 8, lower panel). Relative to observations, all RCMs HIST simulations display underestimation. Quantile–quantile (QQ) plot gives the same results (not shown) and our intensity distribution is equivalent to QQ plot but displaying results only for every 10 percentiles, since intensities are measured based on percentiles. This overall underestimation of PR intensity seems to be mainly due to overestimation of light-rain days in RCMs, and additional contribution might be caused by underestimation for moderate and heavy rain, as presented in the frequency distribution above. Precipitation intensity in the future is expected to increase in every percentile, but its amplitude is stronger in higher precipitation percentiles. In general, five RCMs show good agreement in the future increases (at least four RCMs agree on change sign; not shown). Except for 99th percentile of the GRIMs RCP8.5 result, all RCMs predict increases in the intensity of extreme precipitation above 95th percentile threshold, in spite of difference in projection magnitude of each RCM under two different RCP scenarios, which ranges from 10.7 to 12.6% for RCP4.5 and 8.5–12.6% for RCP8.5 (note percentage change relative to the present-day climate). Also, RCP4.5 scenarios project larger increases than RCP8.5 scenarios, except 98th and 99th percentiles which are “more extreme” cases and will better follow the C–C relationship (Allen and Ingram 2002). This smaller increase in precipitation intensity under a stronger anthropogenic radiative forcing suggests additional contribution of the dynamic effect to the changes in extreme precipitation, which is further examined below.

In summary, RCM projections suggest that while total rain days decrease due mainly to decrease in light rain frequency, heavy rain events occur more frequently with intensified precipitation amount. This corresponds to a shift of precipitation spectrum over South Korea in the future, corroborating previous findings from RCM (Lee et al. 2014; Im et al. 2015; Oh et al. 2016) and GCM studies (Freychet et al. 2015) for East Asia, which would exert

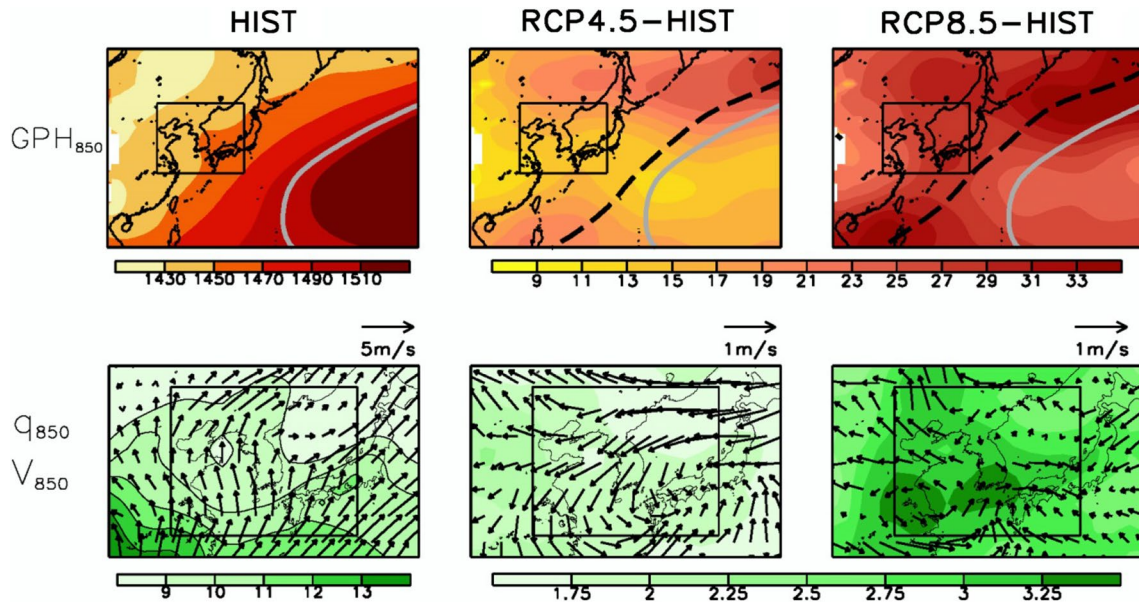


Fig. 6 Spatial distribution of geopotential height (GPH_{850} , unit: meters) and specific humidity (q_{850} , unit: g/kg) and horizontal winds (V_{850} , unit: m/s) at 850 hPa level simulated from the HadGEM2-AO GCM. JJA mean climatology is shown for HIST (left), and future changes relative to the historical period are displayed for RCP4.5

(middle) and RCP8.5 scenarios (right panel). For GPH_{850} , grey solid lines indicate 1500 m contours from HIST and black dashed lines represent those from RCP scenarios. Black boxes indicate the Northeast Asian domain used for RCM simulations

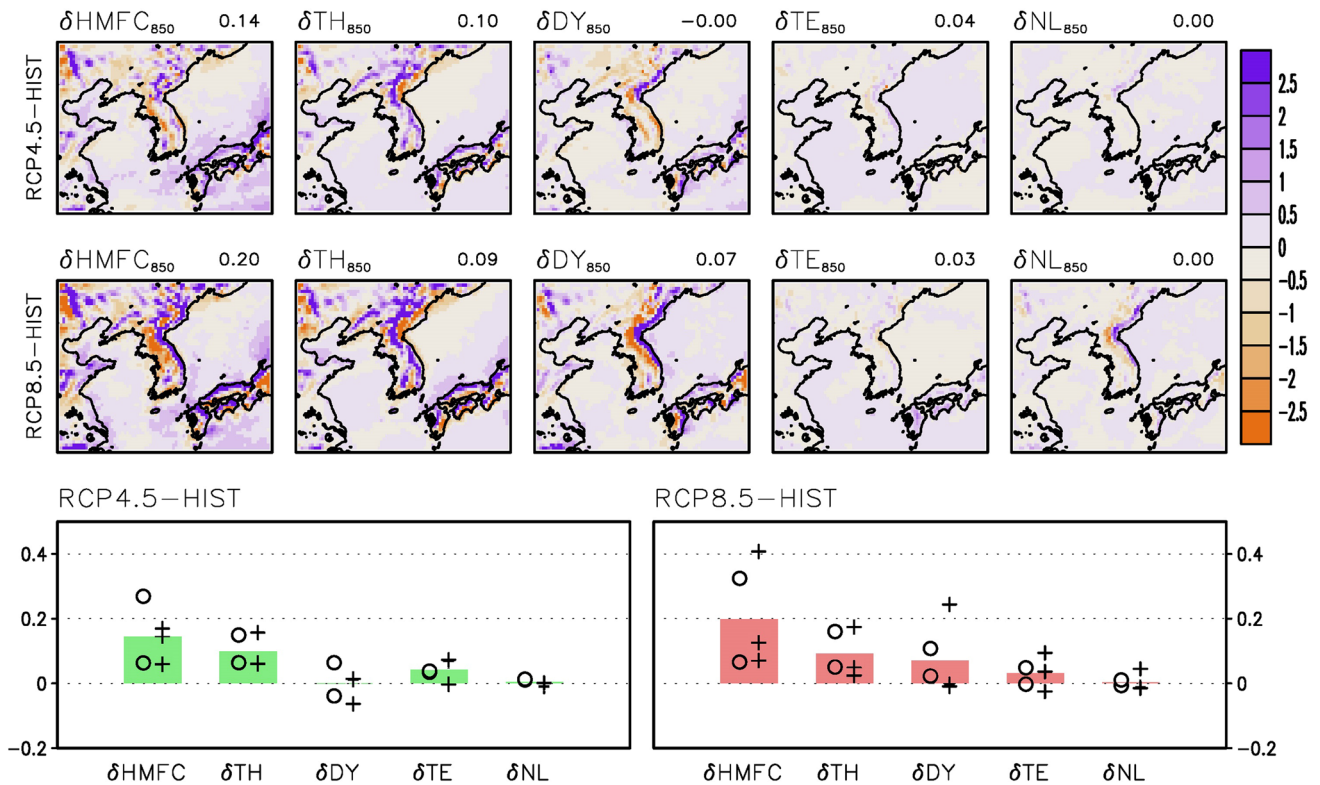
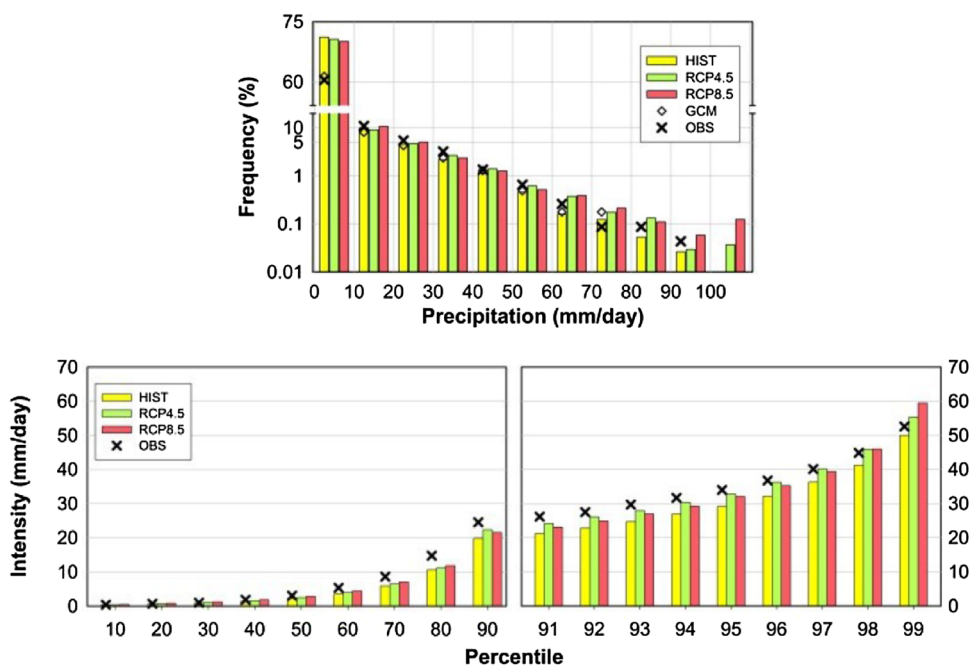


Fig. 7 (Upper) spatial patterns and (lower) Northeast Asian area-averaged changes of 850 hPa horizontal moisture flux convergence ($\delta HMFC$), and thermodynamic (δTH), dynamic (δDY), transient eddy (δTE) and non-linear (δNL) terms contributions (units: $g/kg/s/10^5$) during JJA obtained from five RCM-MME for RCP4.5 and

RCP8.5 scenarios. Numbers on the top of each panel indicate domain averaged value. In the lower panel, bars represent RCM-MME results for RCP4.5 (green) and RCP8.5 (red) scenarios. Results from individual RCMs are indicated with marks (+: RCMs with spectral nudging applied, O: RCMs without spectral nudging)

Fig. 8 (Upper) Frequency (%) distribution of daily PR averaged over South Korea (using wet days with larger than 0.1 mm/day) calculated from observation (APHRODITE), five RCM-MME of HIST, RCP4.5, and RCP8.5 experiments. GCM results are also displayed for comparison. Note near log-scale vertical axis for better comparison of extremes. (lower) Distribution of precipitation intensity (mm/day) measured based on percentiles with 10 bins of every 10 percentiles and also 10 bins of every 1 percentile for the top 10 percentile. See text more details



huge impacts on this region. Larger increases in precipitation under stronger radiative forcing in the RCP8.5 scenario are expected than in the RCP4.5 scenario, but differences in precipitation characteristics between two different scenarios are not big enough to find influence of GHG forcing strength unlike the case of temperature and moisture responses (e.g., Lee et al. 2016).

3.3 Summer extreme precipitation over South Korea

3.3.1 RCM performance

As discussed above, according to RCM projections under RCP scenarios, more frequent heavy rain events are projected to occur over South Korea with extreme precipitation intensity enhanced. For further analysis, extreme precipitation events are defined as days having precipitation above 95th percentile (PR95) for observations and each RCM (Note that only wet days during JJA are considered with daily precipitation averaged over South Korea larger than 0.1 mm/day). For example, from observation data for 1981–2005 summers (JJAs), we find that in total there were 96 days with daily precipitation more than 34 mm/day (PR95 of observations.). Using these dates of extreme precipitation events, we then make composites of variables to examine representative synoptic patterns when extreme precipitation occurs over South Korea. Performance of RCMs in simulating the synoptic patterns is analyzed in comparison with observed patterns.

Figure 9 shows composite patterns of low-level (850 hPa) temperature and humidity and precipitation

obtained from observations and RCM-MME for the days of extreme precipitation over South Korea. Note that in order to better identify warm humid air and cold dry air, we show θ_e at 850 hPa (Hong and Lee 2009; Tomita et al. 2011). RCMs can simulate the observed θ_e pattern of north–south gradient, showing that hotter and more humid air is located to the southwest when extreme precipitation occurs in Korea. However, systematic bias exists such as warm bias in the western part of the domain (up to +8 K) and cold bias over the east ocean area and Japan (around –2 K). The observed composite of 850 hPa humidity and winds displays a well-developed low pressure system located over the Yellow Sea and associated strong south-westerly flow transferring moisture from the East China Sea to the southern part of the Korean Peninsula. RCMs simulate this moisture and wind pattern reasonably well, but south-westerly wind is slightly weaker than the observed and there is a west-wet and east-dry bias in humidity. This systematic west-east bias in humidity is consistent with the θ_e bias pattern. RCM precipitation composites during extreme rains over South Korea are also quite similar to those of observations with a systematic bias of more-intense precipitation in North Korea and less-intense precipitation in South Korea and Kyushu area, which also resembles the bias pattern for mean climate (Fig. 2).

We examine temporal evolution of synoptic patterns in the course of extreme precipitation events over South Korea by compositing variables from 2 day before (–2 day) to 1 day after (+1 day) extreme rain days. HMFC patterns are analyzed in addition to θ_e , specific humidity (q_{850}), and horizontal winds at 850 hPa, and all

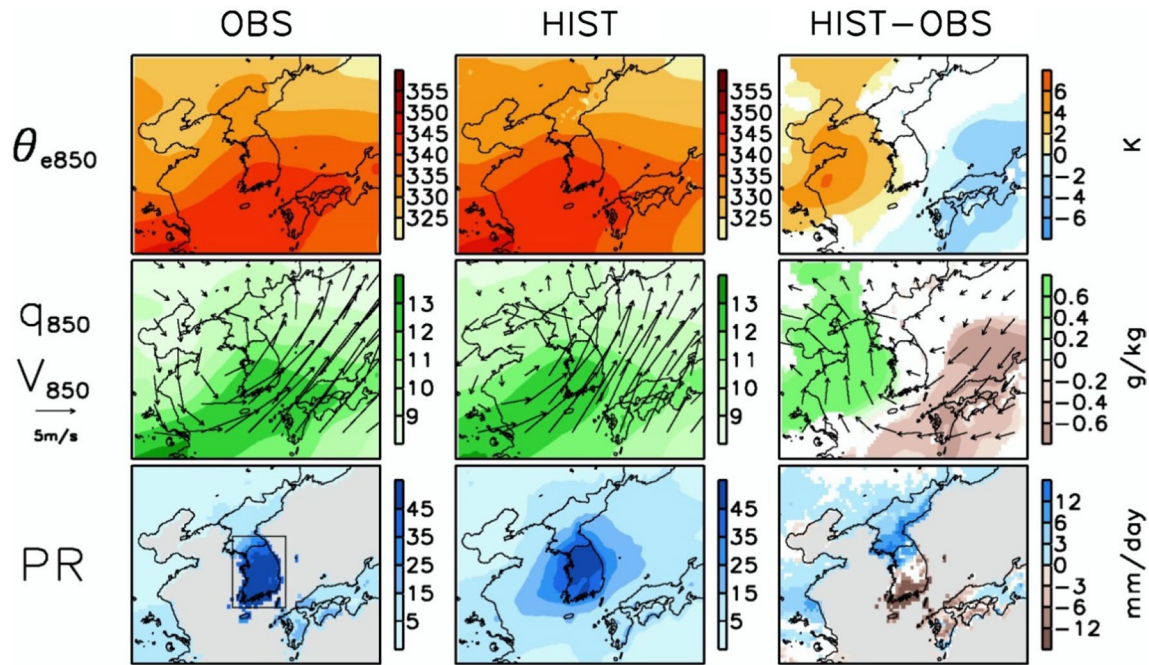


Fig. 9 Composite patterns for extreme precipitation events over South Korea: JJA mean equivalent potential temperature at 850 hPa (θ_{e850} , top), specific humidity at 850 hPa (q_{850}) with horizontal wind vectors (V_{850} , middle), and precipitation (PR, bottom panels) from observations (left), RCM-MME HIST (middle), and RCM-MME bias

(right column). In the bias patterns, shading represents areas with good inter-RCM agreement (at least four agree on the sign of bias). Grey colors in PR depict missing data areas in the APHRODITE observations

results are represented as anomalies relative to the corresponding daily climatology of each data. Figure 10a displays the observed evolution patterns. During 2 days before extreme rain event, anomalous larger amount of moisture is transferred from the south and converges over the Yellow Sea. On extreme rain day, low pressure is situated over South Korea with strong moisture flux convergence. The boundary between cold air mass and warm air mass, which is represented by a strong θ_e gradient, is positioned along South Korea. In +1 day, anomalous low pressure system moves to the northeast, and HMFC and temperature gradient between two air masses becomes weakened. This result suggests that on average, extreme events over South Korea are associated with large-scale low pressure system moving from southwest to northeast. This system is largely consistent with monsoonal (Chang-ma) front that typically brings heavy rain events to Korea during mid-June to late-July, known as the Changma period, and during mid-August to early September, known as the post-Changma period (Kim et al. 2010). Previous studies (Yihui and Chan 2005; Kusunoki et al. 2006; Ham et al. 2015) have examined this large-scale low pressure system over East Asia during summer, which corresponds to the quasi-stationary convergence zone between warm and humid air mass from the south and cold air mass from the north.

It should be noted, however, that there are other weather systems leading to extreme precipitation events over East Asia during summer, including tropical cyclone (typhoon) in late summer and mesoscale disturbances in mid-summer (Yihui and Chan 2005; Kim et al. 2010; Chu et al. 2012). Particularly, in order to check possible influence of tropical cyclone on our composite results, we have redrawn the observed composites using non-typhoon 68 days, i.e. after excluding 28 days when typhoons influenced the Korean Peninsula (KMA 2011), and obtained generally consistent results (not shown). It is hard to separate contribution of mesoscale convective complexes from that of monsoonal front since they intensify closely linked with monsoon front (Yihui and Chan 2005). We also note that synoptic evolution results are based on anomalies relative to each day climatology. Therefore, influence of different weather systems will be partly smoothed out. In short, our composites provide typical synoptic patterns, resembling monsoon system evolutions, but contribution of smaller-scale weather systems needs to be considered with care. This requires a sub-seasonal analysis of weather system (e.g., Chu et al. 2012), which is beyond the scope of this study and will be examined in the future work.

Figure 10b shows evolution of synoptic patterns associated with extreme precipitation in Korea simulated by five RCMs. Extreme events are selected from each RCM

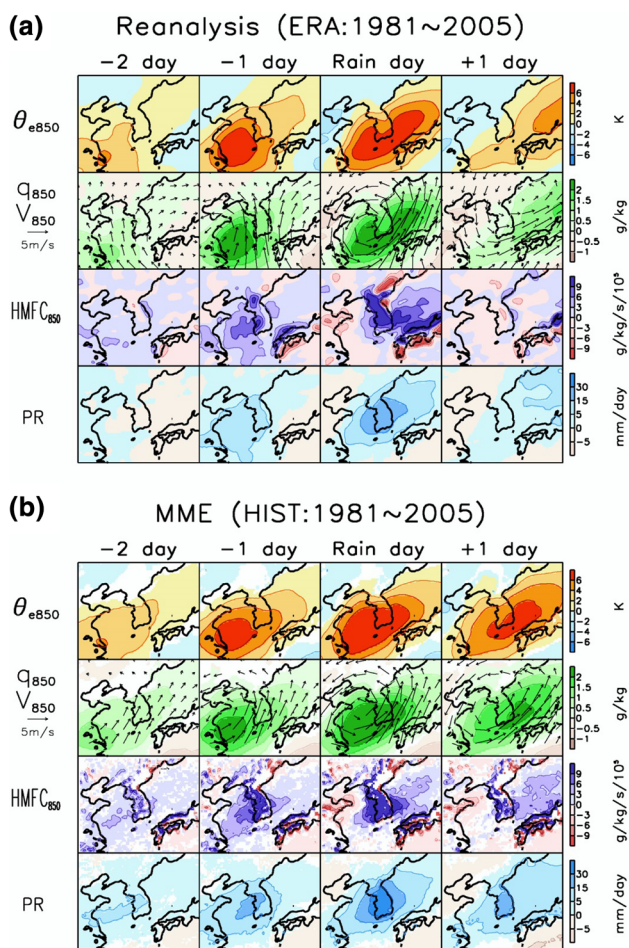


Fig. 10 **a** Evolution of synoptic patterns during extreme precipitation events over South Korea obtained from ERA-interim reanalysis (from 2 days before to 1 day after the event day): Equivalent potential temperature (K), specific humidity (q_{850} , g/kg) with horizontal wind vector (V_{850} , m/s), HMFC at 850 hPa ($g/kg/s/10^5$), and PR (mm/day). Note that all values are anomaly with respect to 1981–2005 mean. **b** Same as **a** except for RCM-MME results from HIST experiment. Shading represents good agreement between RCMs (at least four out of five RCMs agree on the anomaly sign)

and then all synoptic patterns are composited across five RCMs. Although RCMs possess systematic biases in background climate (Fig. 9), models reproduce the observed space–time patterns of large-scale low pressure system development, including the southwest to northwest movement of the system with the location and amplitude of moisture tongue and wind patterns. Some differences from observations are noticeable. The weakening of HMFC after extreme rain day seems to be delayed in RCM results. Also the strong gradient zone of 850 hPa θ_e is positioned slightly to the northwest on rain days in the models. Accordingly, moisture flux convergence zone is shifted northward compared to the observations (Fig. 10). An interesting feature that can be seen from both reanalyses and RCMs is that

HMFC shows similar composite patterns to those of precipitation with larger values confined near South Korea, different from large-scale patterns of moisture and south-westerly winds. This confirms that low-level moisture flux convergence importantly affects precipitation.

3.3.2 Future projection

Future projections of synoptic patterns associated with extreme precipitation over South Korea are examined. Figure 11 shows composite results of future projected patterns and their changes relative to the present composites for RCP4.5 and RCP8.5 scenarios, respectively. Overall patterns of future climates for low-level θ_e , humidity and winds are similar to those of present day composites (Fig. 9) with the warmer and wetter air mass located in the south and the colder and drier one to the north. On the other hand, change patterns in 850 hPa θ_e resemble specific humidity patterns (Fig. 11), indicating that changes in humidity and corresponding changes in latent heat release determine the spatial patterns of θ_e trends. Changes in horizontal winds are much weaker than its absolute climate values, but change patterns of wind vectors follow those of mean climate changes in RCMs (Fig. 5) and in boundary GCM (Fig. 6). As in mean results, there appear different patterns in circulation changes between RCP4.5 and RCP8.5 scenarios, indicating dynamic effect as defined in Eq. (8). RCP4.5 scenario exhibits anomalously cyclonic circulation but RCP8.5 scenario predicts divergent winds over South Korea. Moisture increases are seen over the southern part of the domain from both scenarios, but more strongly in the RCP8.5 scenario, which seems to be due to more warming. Extreme precipitation is expected to increase in the southern Korean Peninsula (around +8.5 and +11.7 mm/day for RCP4.5 and RCP8.5, respectively, averaged over 34°N–37°N) with no change or slight decrease in the central-northern Korean Peninsula (+0.02 and –2.7 mm/day for RCP4.5 and RCP8.5, respectively, using 37°N–40°N). Changes in horizontal wind vectors suggest possible dynamic contribution to the change patterns of precipitation, which is examined below using moisture flux convergence analysis. Although there are some systematic biases in the RCMs (Fig. 9), we find non-significant inter-RCM correlation between model bias and future projection of South Korean extreme precipitation (not shown), indicating possibly weak impacts of model bias on future projections.

Evolution of synoptic system during extreme precipitation days over South Korea is examined from RCP4.5 and RCP8.5 scenarios (Fig. 12). As done for observations and HIST simulations (Fig. 10), all variables are expressed as anomalies relative to their respective future climatology. Results show that monsoonal front system is expected to continue to occur in the future during extreme precipitation

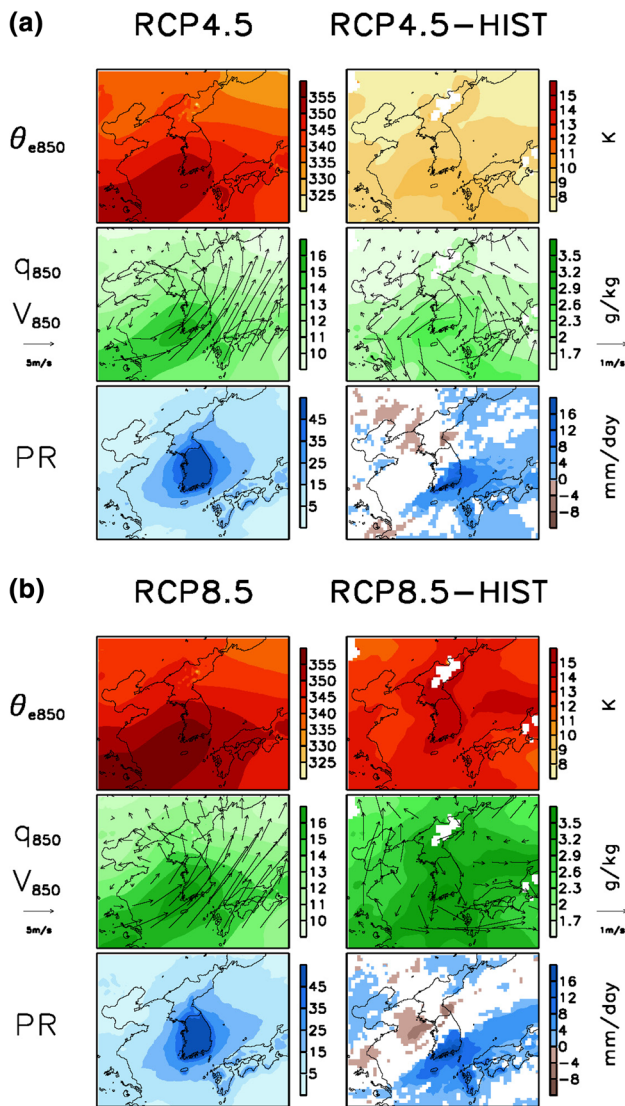


Fig. 11 **a** Future climate patterns (*left*) during extreme precipitation days over South Korea obtained from 5 RCM-MME simulations under RCP4.5 scenario, and their change patterns (*right*) relative to HIST results for equivalent potential temperature (K) and specific humidity (q_{850} , g/kg) with horizontal winds (V_{850} , m/s) at 850 hPa, and PR (mm/day). **b** Same as **a** except for RCP8.5 scenario. In climate change patterns, *shading* represents region where at least four out of five RCMs agree on the change sign

days. Patterns of θ_e anomaly suggest a slight southward shift of the frontal zone between cold and warm air masses in the future, but the inter-RCM uncertainty is quite large as indicated by white areas.

Extreme precipitation events are likely to occur more frequently and with larger strengths under global warming on average as shown above (Sect. 3.2). Also background warming and moistening are projected to occur with different strengths according to different radiative greenhouse-gas forcing (Fig. 11). However, when comparing

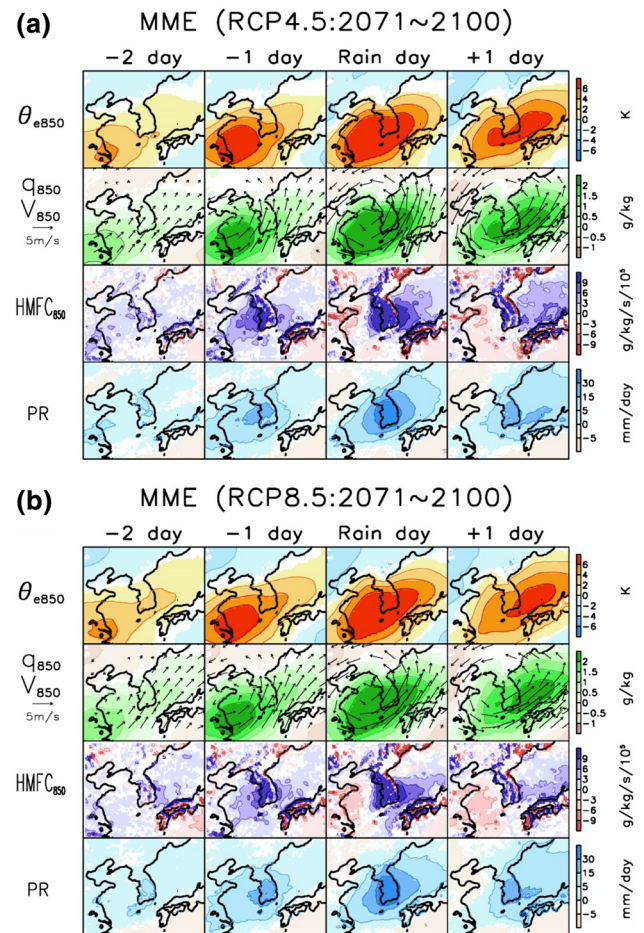


Fig. 12 Same as Fig. 10b except for **a** RCP4.5 and **b** RCP8.5 scenarios, respectively. Note that all values are anomaly with respect to 2071–2100 mean

anomalous synoptic pattern evolutions related to extreme precipitation between two RCP scenarios, they are found to be similar to each other and also to the present day patterns (Fig. 12). Here our study focused on understanding evolution of typical synoptic anomaly patterns associated with extreme precipitation over South Korea, but investigating changes in frequency of low pressure system would also be needed with different types and intensities considered, which requires further analysis using cyclone classification techniques over larger area (cf. Chu et al. 2012).

3.3.3 Thermodynamic and dynamic contributions

Results shown above (Fig. 11) suggest possible roles of changes in atmospheric circulation pattern as well as the background moisture increase due to warming in determining future changes in extreme precipitation over Korea. In order to quantify relative contributions of the dynamic (DY) and thermodynamic (TH) effects on

extreme precipitation changes, we apply $HMFC_{850}$ analysis using horizontal winds and moisture fields during extreme precipitation days that have been selected based on the PR95 threshold (see above). Figure 13 shows the results for RCP4.5 and RCP8.5 scenario runs. Total changes in $HMFC_{850}$ show different responses between scenarios. RCP4.5 scenario shows overall increase in $HMFC$ over South Korea, but decrease in moisture convergence is dominant over the central part of the Korean Peninsula in the RCP8.5 scenario. Spatial patterns between $HMFC_{850}$ changes and extreme precipitation changes (Fig. 12) are similar. As discussed above, composites during extreme precipitation events will more clearly display strong moisture convergences, because no-rain and little-rain days are excluded, when divergence will contribute to $HMFC$ reduction depending on regions.

Spatial patterns of TH and DY contributions (Fig. 13) demonstrate that TH effect increases in moisture convergence over Korea for both RCP scenarios. In contrast, DY effect plays a role in decreasing moisture convergence in this region, more strongly in the RCP8.5 scenario. Therefore, the drying trends in future extreme precipitation turn out to be due to atmospheric circulation changes, which offset thermodynamic moistening effect, as in the case of Northeast Asian mean precipitation (Fig. 7).

Area (South Korea) averaged $HMFC_{850}$ changes are compared with TH and DY contributions during extreme precipitation events over South Korea (Fig. 13, bottom). All RCMs show positive contribution by TH effects but DY effects are different across RCMs. Hence, uncertainty in $HMFC_{850}$ change mainly arises from the uncertainty in DY effect, as in the case of Northeast Asian mean precipitation (Fig. 7). This implies that uncertainty in extreme precipitation is also affected by DY projection uncertainty, which is in accord with previous findings based on GCM studies (Endo and Kitoh 2014). We find that the influence of δTE and δNL terms is generally negligible as in Northeast Asian mean changes (Fig. 7). One exception is considerable contribution of δNL to extreme PR changes in RCP8.5 scenario. In addition, there might be possible impacts of spectral nudging on extreme precipitation changes with some differences identified in DY and NL terms between models with + mark with those with O mark (Fig. 13), which requires further investigation.

3.4 Summary and discussion

This study examines space–time patterns of future precipitation changes over the Northeast Asia and South Korea during summer season (June–July–August, JJA)

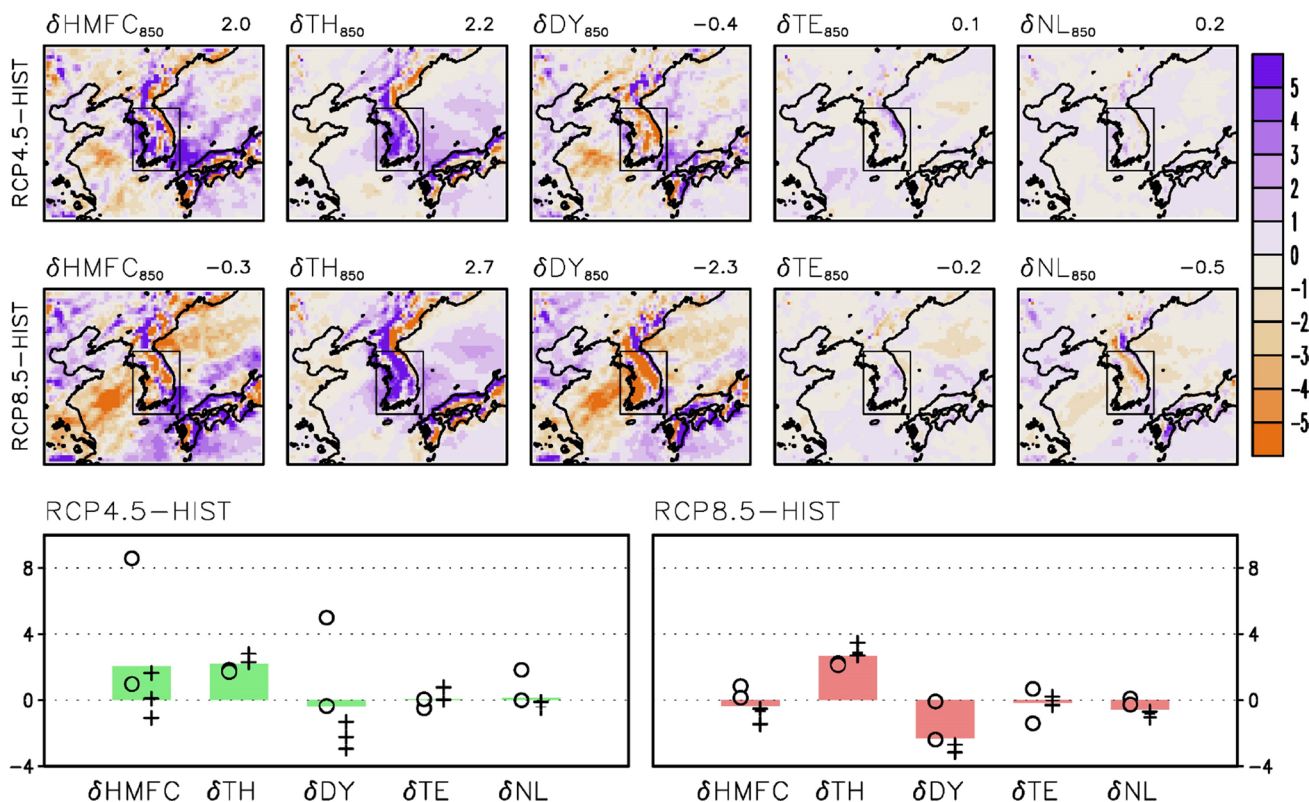


Fig. 13 Same as Fig. 7 except for composites during extreme precipitation days. Numbers on the top of each panel represent areas mean values for South Korea (box region)

using five RCMs driven by single GCM under two different RCP scenarios. Future changes in mean precipitation over the Northeast Asia and extreme precipitation over South Korea are assessed together with related changes in temperature, humidity, and winds. In particular, physical mechanisms responsible for precipitation changes are explored by analyzing moisture flux convergence at 850 hPa, which are found to be closely related to precipitation, and its thermodynamic (TH) and dynamic (DY) components. Results from two future emission scenarios are also compared to investigate influence of external radiative forcing on future precipitation characteristics. Main findings from our analyses are summarized as follows.

- Five RCMs driven by single GCM boundary forcing show good agreements in both biases and future projections in mean climate, indicating the major influence of driving GCM. The consistent patterns of low-level winds across RCMs (in addition to temperature and moisture) suggest that this inter-RCM agreement is partly due to spectral nudging applied in three RCMs.
- Future projections show warmer and more humid climate everywhere over the Northeast Asia and the area-averaged increase in atmospheric moisture is found to be consistent with the C–C relationship (~7% increase per 1 °C warming). This overall background moistening induces the positive contribution of the TH effect to future change in moisture flux convergences and precipitation.
- According to RCM projections, mean precipitation is expected to increase over a large part of the Northeast Asia, majorly due to TH contribution of horizontal moisture flux convergence increase under warming. However, it is also demonstrated that DY contribution involving atmospheric circulation changes can affect precipitation changes, offsetting the TH contribution in some regions such as the central part of the Korean Peninsula. This DY effect can induce local divergence of horizontal moisture flux, resulting in no change or slight decrease in precipitation.
- RCMs overall project increases in both frequency and intensity of extreme precipitation over South Korea, which will exert more harm to human society and the ecosystem. Extreme precipitation over the central part of Korean Peninsula is expected to decrease as in the mean precipitation change. Composite analysis shows that the extreme precipitation events in both present and future periods mainly involve the evolution of large-scale low-pressure system. This synoptic pattern is analyzed to move along the monsoonal (Chang-ma) front that corresponds to the boundary between the warm and humid air mass and the cold air mass.
- RCP4.5 and RCP8.5 scenarios show different change patterns of extreme precipitation over South Korea, which is caused by differences in DY contribution. Despite of larger positive TH effect, much larger negative contribution of DY effect in the RCP8.5 scenario makes non-significant difference between two scenarios. This uncertainty in dynamic projections explains most of the uncertainty in HMFC change. This highlights the important role of atmospheric circulation changes in determining local responses in extreme precipitation, which should be further studied.

Our results on Northeast Asian precipitation changes provide important implications for the Asian monsoon and other monsoon regions. The distinct characteristics of change in precipitation over Asia region were investigated by several CMIP5 studies. Kitoh et al. (2013) reveals that the frequency of precipitating events decreases as the atmosphere stabilizes, but projected changes in extreme precipitation intensities over Asian monsoon regions are larger than other regions, implying that sensitivity of Asian monsoon to global warming is stronger than that of other regional monsoons. Endo and Kitoh (2014) showed that positive contribution of TH is consistently projected by CMIP5 in every monsoon region, supporting CMIP3-based results (Seager et al. 2010). However, in regional scale, negative contribution of DY can offset or overwhelm TH contribution, which eventually determines change in regional precipitation. Interestingly, CMIP5 projections in DY term generally have good agreement except for three regions, South Asia, Western-north Pacific and East Asia where are under impacts of WNPSH. In this respect, He and Zhou (2015) pointed a large uncertainty in future WNPSH and its impacts on EASM among CMIP5 models, showing that the MME projected changes in WNPSH intensity are approximately zero due to large cancellation among different projections from different models. This emphasizes the importance of the uncertainty factors associated with WNPSH, consistent with our findings from the Northeast Asia, requiring further analyses using multi-model ensembles.

Relative contributions to uncertainties prevailed in RCM projections (e.g. scenario, boundary GCM, RCM, internal variability) has recently been reviewed by Giorgi and Gutowski (2016). Particularly, the difference in RCM physics was suggested to importantly affect local projections like summer convective precipitation, even when driven by the same GCM boundary conditions. Therefore, in order to reduce uncertainty arising from DY effect in local precipitation changes, one needs to improve models for more reliable simulations of each air mass and their interactions as well as for their capability of reproducing both large-scale (GCM) and local-scale (RCM) physical processes.

This study provides the first mechanism analysis for Northeast Asia and South Korea region using multiple RCMs with systematic investigation of TH and DY contribution to precipitation change. However, there is a caveat in this study due to the use of single driving GCM. Since RCMs are strongly governed by boundary forcing GCM in this region, RCM outputs is likely to be influenced by systematic biases of the driving GCM. This will limit full consideration of inter-model uncertainties in assessing the future projection uncertainties. For more reliable projection of extreme precipitation change and assessment of its physical mechanisms, it is fundamental to consider uncertainty factors more comprehensively by including inter-GCM differences. Also, sub-seasonal precipitation system in EASM needs to be considered in assessing future projections of sub-regional precipitation changes (e.g., central vs. southern region Changma, or Meiyu-Changma-Baiu comparisons), particularly to identify distinct physical mechanisms responsible for the smaller-scale changes in different sub-seasons (e.g., Chu et al. 2012; Oh and Ha 2016).

Acknowledgements Authors thank Jong-Seong Kug and two anonymous reviewers for their clarifying and constructive comments. This work was supported by the Korea Meteorological Administration Research and Development Program under Grant KMIPA 2015–2082. The computational resource and corresponding technical solutions were supported by Korea Institute of Science and Technology Information (Project No. KSC-2014-G3-006). Ji-Woo Lee is supported by the U.S. Department of Energy Office of Science/Office of Biological and Environmental Research under Contract DE-AC52-07NA27344 at Lawrence Livermore National Laboratory.

References

- Ahn J-B, Jo S, Suh M-S et al (2016) Changes of precipitation extremes over South Korea projected by the 5 RCMs under RCP scenarios. *Asia Pac J Atmos Sci* 52:223–236
- Allan RP (2009) Examination of relationships between clear-sky longwave radiation and aspects of the atmospheric hydrological cycle in climate models, reanalyses, and observations. *J Clim* 22:3127–3145
- Allen MR, Ingram WJ (2002) Constraints on future changes in climate and the hydrologic cycle. *Nature* 419:224–232
- Baek H-J, Lee J, Lee H-S et al (2013) Climate change in the 21st century simulated by HadGEM2-AO under representative concentration pathways. *Asia Pac J Atmos Sci* 49:603–618
- Cha D-H, Jin C-S, Moon J-H, Lee D-K (2015) Improvement of regional climate simulation of East Asian summer monsoon by coupled air–sea interaction and large-scale nudging. *Int J Climatol*. doi:10.1002/joc.4349
- Cha D-H, Lee D-K, Jin C-S et al (2016) Future changes in summer precipitation in regional climate simulations over the Korean peninsula forced by multi-RCP scenarios of HadGEM2-AO. *Asia Pac J Atmos Sci* 52:139–149
- Choi Y-W, Ahn J-B, Suh M-S et al (2016) Future changes in drought characteristics over South Korea using multi regional climate models with the standardized precipitation index. *Asia Pac J Atmos Sci* 52:209–222
- Chu J-E, Hameed SN, Ha K-J et al (2012) Nonlinear, intraseasonal phases of the East Asian summer monsoon: extraction and analysis using self-organizing maps. *J Clim* 25:6975–6988
- Dee DP, Uppala SM, Simmons AJ et al (2011) The ERA-Interim reanalysis: configuration and performance of the data assimilation system. *Q J R Meteorol Soc* 137:553–597. doi:10.1002/qj.828
- Deser C, Phillips AS, Alexander MA, Smoliak BV (2014) Projecting north American climate over the next 50 years: uncertainty due to internal variability. *J Clim* 27:2271–2296
- Di Luca A, de Elía R, Laprise R (2015) Challenges in the quest for added value of regional climate dynamical downscaling. *Curr Clim Change Rep* 1:10–21
- Emori S, Brown SJ (2005) Dynamic and thermodynamic changes in mean and extreme precipitation under changed climate. *Geophys Res Lett* 32:L17706. doi:10.1029/2005GL023272
- Endo H, Kitoh A (2014) Thermodynamic and dynamic effects on regional monsoon rainfall changes in a warmer climate. *Geophys Res Lett* 41:1704–1711. doi:10.1002/2013GL059158
- Freychet N, Hsu HH, Chou C, Wu CH (2015) Asian summer monsoon in CMIP5 projections: a link between the change in extreme precipitation and monsoon dynamics. *J Clim* 28:1477–1493
- Gao Y, Leung LR, Salathé Jr EP, Dominguez F, Nijssen B, Lettenmaier DP (2012) Moisture flux convergence in regional and global climate models: implications for droughts in the southwestern United States under climate change. *Geophys Res* 39:L09711 doi:10.1029/2012GL051560
- Giorgi F, Gutowski WJ (2016) Coordinated experiments for projections of regional climate change. *Curr Clim Change Rep* doi:10.1007/s40641-016-0046-6
- Giorgi F, Jones C, Asrar GR (2009) Addressing climate information needs at the regional level: the CORDEX framework. *WMO Bull* 58:175–183
- Giorgi F, Coppola E, Solmon F et al (2012) RegCM4: model description and preliminary tests over multiple CORDEX domains. *Clim Res* 52:7–29. doi:10.3354/cr01018
- Ham S, Lee J-W, Yoshimura K (2015) Assessing future climate changes in the East Asian summer and winter monsoon using Regional Spectral Model. *J Meteor Soc Jpn*. doi:10.2141/jmsj.2015-051
- He C, Zhou T (2015) Responses of the Western North Pacific subtropical high to global warming under RCP4.5 and RCP8.5 scenarios projected by 33 CMIP5 models: the dominance of tropical Indian Ocean—tropical Western Pacific SST gradient. *J Clim* 28:365–380. doi:10.1175/JCLI-D-13-00494.1
- Held IM, Soden BJ (2006) Robust responses of the hydrological cycle to global warming. *J Clim* 19:5686–5699
- Hewitt HT, Copsey D, Culverwell, I. D et al (2011) Design and implementation of the infrastructure of HadGEM3: the next-generation Met Office climate modelling system. *Geosci Model Dev* 4:223–253. doi:10.5194/gmd-4-223-2011
- Hong J-Y, Ahn J-B (2015) Changes of early summer precipitation in the Korean Peninsula and nearby regions based on RCP simulations. *J Clim* 28:3557–3578
- Hong S-Y, Chang E-C (2012) Spectral nudging sensitivity experiments in a regional climate model. *Asia Pac J Atmos Sci* 48:345–355
- Hong S-Y, Kanamitsu M (2014) Dynamical downscaling: Fundamental issues from an NWP point of view and recommendations. *Asia Pac J Atmos Sci* 50:83–104. doi:10.1007/s13143-014-0029-2
- Hong S-Y, Lee J-W (2009) Assessment of the WRF model in reproducing a flash-flood heavy rainfall event over Korea. *Atmos Res* 93:818–831. doi:10.1016/j.atmosres.2009.03.015
- Hong S-Y, Park H, Cheong H-B et al (2013) The global/regional integrated model system (GRIMs). *Asia Pac J Atmos Sci* 49:219–243. doi:10.1007/s13143-013-0023-0

- Im E-S, Ahn J-B, Jo S-R (2015) Regional climate projection over South Korea simulated by the HadGEM2-AO and WRF model chain under RCP emission scenarios. *Clim Res* 63:249–266. doi:[10.3354/cr01292](https://doi.org/10.3354/cr01292)
- IPCC (2013) Climate Change 2013: The Physical Science Basis. In: Stocker TF et al (eds) Contribution of Working Group I to the Fifth Assessment Report of the Intergovernmental Panel on Climate Change. Cambridge University Press, Cambridge
- Kalnay E, Kanamitsu M, Kistler R et al (1996) The NCEP/NCAR 40-year reanalysis project. *Bull Am Meteorol Soc* 77:437–470
- Kanamaru H, Kanamitsu M (2007) Scale-selective bias correction in a downscaling of global analysis using a regional model. *Mon Weath Rev* 135:334–350
- Kendon EJ, Rowell DP, Jones RG (2010) Mechanisms and reliability of future projected changes in daily precipitation. *Clim Dyn* 35:489–509 doi:[10.1007/s00382-009-0639-z](https://doi.org/10.1007/s00382-009-0639-z)
- Kharin VV, Zwiers FW, Zhang X, Hegerl GC (2007) Changes in temperature and precipitation extremes in the IPCC ensemble of global coupled model simulations. *J Clim* 20:1419–1444. doi:[10.1175/JCLI4066.1](https://doi.org/10.1175/JCLI4066.1)
- Kim K-Y, Roh J-W, Lee D-K, Jhun J-G (2010) Physical mechanisms of the seasonal, subseasonal, and high-frequency variability in the seasonal cycle of summer precipitation in Korea. *J Geophys Res* 115:D14110. doi:[10.1029/2009JD013561](https://doi.org/10.1029/2009JD013561)
- Kitoh A, Endo H, Krishna Kumar K, Cavalcanti IFA, Goswami P, Zhou T (2013) Monsoons in a changing world: a regional perspective in a global context. *J Geophys Res Atmos* 118:3053–3065. doi:[10.1002/jgrd.50258](https://doi.org/10.1002/jgrd.50258)
- KMA (2011) Typhoon White Book, National Typhoon Center, Korea Meteorological Administration, pp 345
- Kusunoki S, Yoshimura J, Yoshimura H, Noda A, Oouchi K, Mizuta R (2006) Change of Baiu rain band in global warming projection by an atmospheric General Circulation Model with a 20-km grid size. *J Meteor Soc Jpn* 84:581–611
- Laprise R (2008) Regional climate modelling. *J Com Phys* 227:3641–3666
- Lee J-W, Hong S-Y (2014) Potential for added value to downscaled climate extremes over Korea by increased resolution of a regional climate model. *Theor Appl Climatol* 117:667–677
- Lee J-Y, Wang B (2014) Future change of global monsoon in the CMIP5. *Clim Dyn* 42:101–119. doi:[10.1007/s00382-012-1564-0](https://doi.org/10.1007/s00382-012-1564-0)
- Lee D-K, Cha D-H, Kang H-S (2004) Regional climate simulation of the 1998 summer flood over East Asia. *J Meteor Soc Jpn* 82:1735–1753
- Lee J-W, Hong S-Y, Chang E-C, Suh M-S, Kang H-S (2014) Assessment of future climate change over East Asia due to the RCP scenarios downscaled by GRIMs-RMP. *Clim Dyn* 42:733–747
- Lee D, Min S-K, Park C et al (2016) Time of emergence of anthropogenic warming signals in the Northeast Asia assessed from multi-regional climate models. *Asia Pac J Atmos Sci* 52:129–137
- Li L, Li W, Kushnir Y (2012a) Variation of the North Atlantic subtropical high western ridge and its implication to Southeastern US summer precipitation. *Clim Dyn* 39:1401–1412
- Li W, Li L, Ting M, Liu Y (2012b) Intensification of northern hemisphere subtropical highs in a warming climate. *Nature Geosci* 5:830–834
- Lin II, Chan JCL (2015) Recent decrease in typhoon destructive potential and global warming implications. *Nature Commun* 6: 7182. doi:[10.1038/ncomms8182](https://doi.org/10.1038/ncomms8182).
- Matsumura S, Sugimoto S, Sato T (2015) Recent intensification of the western Pacific subtropical high associated with the East Asian summer monsoon. *J Clim* 28:2873–2883
- Miguez-Macho G, Stenchikov GL, Robock A (2004) Spectral nudging to eliminate the effects of domain position and geometry in regional climate model simulations. *J Geophys Res* 109:D13104
- Min S-K, Legutke S, Hense A, Cubasch U, Kwon W-T, Oh J-H, Schlese U (2006) East Asian climate change in the 21st century as simulated by the coupled climate model ECHO-G under IPCC SRES scenarios. *J Meteor Soc Jpn* 84:1–26
- Min S-K, Zhang X, Zwiers FW, Hegerl GC (2011) Human contribution to more-intense precipitation extremes. *Nature* 470:378–381
- Min S-K, Son S-W, Seo K-H et al (2015) Changes in weather and climate extremes over Korea and possible causes: a review. *Asia Pac J Atmos Sci* 51:103–121
- Murphy J (1999) An evaluation of statistical and dynamical techniques for downscaling local climate. *J Clim* 12:2256–2284
- O’Gorman PA, Schneider T (2009) The physical basis for increases in precipitation extremes in simulations of 21st-century climate change. *Proc Natl Acad Sci USA* 106:14773–14777
- Oh H and Ha K-J (2016) Prediction of dominant intrapersonal modes in the East Asian-western North Pacific summer monsoon. *Clim Dyn* 47:2025–2037
- Oh S-G, Suh M-S, Cha D-H (2013) Impact of lateral boundary conditions on precipitation and temperature extremes over South Korea in the CORDEX regional climate simulation using RegCM4. *Asia Pac J Atmos Sci* 49:497–509
- Oh S-G, Suh M-S, Lee Y-S et al (2016) Projections of high resolution climate changes for South Korea using multiple-regional climate models based on four RCP scenarios. Part 2: precipitation. *Asia Pac J Atmos Sci*. doi:[10.1007/s13143-016-0018-8](https://doi.org/10.1007/s13143-016-0018-8)
- Park C, Min S-K, Lee D et al (2016) Evaluation of multiple Regional Climate Models for summer climate extremes over East Asia. *Clim Dyn* 46:2469–2486. doi:[10.1007/s00382-015-2713-z](https://doi.org/10.1007/s00382-015-2713-z)
- Seager R, Henderson N (2013) Diagnostic computation of moisture budgets in the ERA-Interim reanalysis with reference to analysis of CMIP-archived atmospheric model data. *J Clim* 26:7876–7901
- Seager R, Naik N, Vecchi GA (2010) Thermodynamic and dynamic mechanisms for large-scale changes in the hydrological cycle in response to global warming. *J Clim* 23:4651–4668
- Seo K-H, Ok J, Son J-H, Cha D-H (2013) Assessing future changes in the East Asian summer monsoon using CMIP5 coupled models. *J Clim* 26:7662–7675
- Skamarock WC, Klemp JB, Dudhia J, Gill DO, Barker DM, Wang W, Powers JG (2005) A description of the advanced research WRF version 2. NCAR Technical Note 468, Mesoscale and Microscale Meteorology Division at NCAR, Boulder
- Stephens GL, Ellis TD (2008) Controls of global-mean precipitation increases in global warming GCM experiments. *J Clim* 21:6141–6155
- Suh M-S, Oh S-G, Lee Y-S et al (2016) Projection of high resolution climate change for South Korea using multiple-regional climate models based on four RCP scenarios. Part 1. Surface air temperature. *Asia Pac J Atmos Sci*. doi:[10.1007/s13143-016-0017-9](https://doi.org/10.1007/s13143-016-0017-9)
- Tomita T, Yamaura T, Hashimoto T (2011) Interannual variability of the Baiu season near Japan evaluated from the equivalent potential temperature. *J Meteor Soc Jpn* 89:517–537
- Trenberth KE, Dai A, Rasmussen RM, Parsons DB (2003) The changing character of precipitation. *Bull Am Meteorol Soc* 84:1205–1217
- Wang B, Wu R, Lau KM (2001) Interannual variability of the Asian summer monsoon: contrasts between the Indian and the Western North Pacific-East Asian Monsoons. *J Clim* 14:4073–4090
- Wilby RL, Wigley TML, Conway D, Jones PD, Hewitson BC, Main J, Wilks DS (1998) Statistical downscaling of general circulation model output: a comparison of methods. *Water Resour Res* 34:2995–3008
- Yang B, Qian Y, Lin G, Leung R, Zhang Y (2012) Some issues in uncertainty quantification and parameter tuning: a case study of convective parameterization scheme in the WRF regional climate model. *Atmos Chem Phys* 12:2409–2427

- Yatagai A, Kamiguchi K, Arakawa O, Hamada A, Yasutomi N, Kitoh A (2012) APHRODITE: constructing a long-term daily gridded precipitation dataset for Asia based on a dense network of rain gauges. *Bull Am Meteorol Soc* 93:1401–1415
- Yihui D, Chan JC (2005) The East Asian summer monsoon: an overview. *Meteor Atmos Phys* 89:117–142
- Yun K-S, Ha K-J, Yeh S-W, Wang B, Xiang B (2015) Critical role of boreal summer North Pacific subtropical highs in ENSO transition. *Clim Dyn* 44: 1979–1992
- Zhang X, Wan H, Zwiers FW, Hegerl GC, Min S-K (2013) Attributing intensification of precipitation extremes to human influence. *Geophys Res Lett* 40:5252–5257
- Zhou T, Yu R, Zhang J et al (2009) Why the western Pacific subtropical high has extended westward since the late 1970s. *J Clim* 22:2199–2215